Thermal Phase Evolution of Pt−Si Intermetallic Thin Films Prepared by the Activated Adsorption of SiH_4 on Pt(100) and Comparison to Known Structural Models

Joseph C. Bondos, Nicole E. Drummer, Andrew A. Gewirth,* and Ralph G. Nuzzo*

Contribution from the School of Chemical Sciences and the Frederick Seitz Materials Research Laboratory, University of Illinois, Urbana, Illinois 61801

Received August 10, 1998

Abstract: We have investigated the growth, morphology, and phase evolution of Pt−Si intermetallic thin films using scanning tunneling microscopy (STM), low-energy electron diffraction (LEED), and Auger electron spectroscopy (AES). These materials were formed through an "inverted" CVD deposition process that involves the exposure of a Pt(100) crystal to silane (SiH^4) followed by flash annealing treatments. Structural studies performed as a function of the annealing temperature reveal a complicated phase behavior that involves the sequential formation of four atomically ordered phases with multilevel character. The nature of this process is analyzed to obtain information about the primary structure-determining interactions responsible for the phase transformations seen in this system. We describe the structure-determining influences seen on the Pt(100) surface and provide a comparison with earlier results obtained on Pt(111) and Ni surfaces. The substrate effects are marked and the differences between the results obtained on Pt(100) and Pt(111) are discussed in detail. A model is presented that relates the structure of the phases obtained on the Pt(100) surface to known bulk Pt silicide phases. Of particular interest is the finding that "inverted" CVD via the thermolytic decomposition of SiH_4 on the Pt(100) substrate yields, upon suitable thermal treatment, a $(\sqrt{17}\times\sqrt{17})R14.0°$ overlayer structure exhibiting two chiral surface domains. This multilayer structure is well described by a termination of the bulk Pt−Si intermetallic phase that is isomorphic with the well-known $Ni_{12}P_5$ structure.

I. Introduction

Metal−semiconductor thin films, especially the silicides, are of fundamental importance in the microelectronics industry.[1,2] Transition metal silicides have been widely used as interconnects, gates in field-effect transistors (FETs), Schottky barriers, and Ohmic contacts in very large scale integration (VLSI) technologies.[1−3] More recently, Pt−Si/Si Schottky diodes (with barrier heights in the 0.79 to 0.88 eV range depending on the Pt−Si stoichiometry[2]) have emerged as an important class of infrared detector with sensitivity in the 3−5 μm wavelength range.[4]

As microelectronic device dimensions have decreased, knowledge of the structure, physical properties, and reactivity of these metal−semiconductor thin films is becoming increasingly important to optimize both fabrication procedures and device performance. Furthermore, with the increasingly smaller device dimensions comes a need to understand these properties at increasingly smaller length scales. It is widely appreciated, for example, that thin film reactions exhibit nonequilibrium phase behavior that is strongly dependent on the interfacial reaction kinetics.[1,2,3,5−8] In part for this reason, the investigation of the structure and properties of the Pt−Si interface has assumed a position of great importance, with the hope that such studies will help to establish which interactions control the underlying phase growth properties.

Most studies of the reactions occurring at the metal−semiconductor interface involve the deposition of thin metal films (<1 μm) on a semiconductor substrate (usually single-crystalline silicon) surface. The metal deposition is then followed by various annealing treatments and the solid−solid reactions ensue either directly or through a thin oxide layer.[1−16] Such processing can result in the formation of a largely uniform intermetallic thin film via solid−solid interdiffusion.[5−7] For example, annealing an ∼100 nm thick film of Pt deposited on a silicon substrate to ca. 573 K initially results in the formation of a uniform Pt_2Si phase.[5−7] At first glance, this result may appear somewhat surprising given that the binary alloy phase

(1) Tu, K. N.; Mayer, J. W. Silicide Formation. In *Thin Films−Interdiffusion and Reactions*; Poate, J. M., Tu, K. N., Mayer, J. W., Eds.; John Wiley & Sons: New York, 1978; pp 359−405.
(2) Mayer, J. W.; Lau, S. S. *Electronic Materials Science: For Integrated Circuits in Si and GaAs*; Macmillan: New York, 1990; p 275.
(3) Muraka, S. P. *Silicides for VLSI Applications*; Academic Press: New York, 1993.
(4) Sandersreed, J. N. *Opt. Eng.* **1997**, *36*, 235.
(5) Ottaviani, G. *J. Vac. Sci. Technol.* **1979**, *16*, 1112.
(6) Ottaviani, G. *J. Vac. Sci. Technol.* **1981**, *18*, 924.
(7) Canali, C.; Majni, G.; Ottaviani, G.; Celotti, G. *J. Appl. Phys.* **1979**, *50*, 255.
(8) Pretorius, R. *Thin Solid Films* **1996**, *290−291*, 477.
(9) Rossi, G. *Surf. Sci.* **1987**, *7*, 1.
(10) Morgen, P.; Szymonski, M.; Onsgaard, B.; Jørgensen, B. *Surf. Sci.* **1988**, *197*, 347.
(11) Itoh, H.; Narui, S.; Sayama, A.; Ichinokawa, T. *Phys. Rev. B* **1992**, *45*, 11136.
(12) Das, S. R.; Sheergar, K.; Xu, D.-X.; Naem, A. *Thin Solid Films* **1994**, *253*, 467.
(13) Colgan, E. G. *J. Mater. Res.* **1995**, *10*, 1953.
(14) Hsu, D. S. Y.; Troilo, L. M.; Turner, N. H.; Pierson, K. W. *Thin Solid Films* **1995**, *269*, 21.
(15) Ley, L.; Wang, Y.; Nguyen, V.; Fisson, S.; Souche, D.; Vuye, G.; Rivory, J. *Thin Solid Films* **1995**, *270*, 561.
(16) Lifshits, V. G.; Saranin, A. A.; Zotov, A. V. *Surface Phases on Silicon. Preparation, Structures, and Properties*; John Wiley & Sons: New York, 1994.

10.1021/ja9828511 CCC: $18.00
Published on Web 03/06/1999

diagram shows the presence of at least five stable phases for this system at this temperature.[17] With continued heating, and only after depletion of the starting Pt_2Si phase, the more silicon rich phase, PtSi, grows.[5−7] The sequential nature of this growth process stems from the relative thinness of the film (∼100 nm) and the interfacial reaction kinetics which together limit the ability of multiple phases to coexist.[2] In direct contrast to the formation of silicides on semiconductor surfaces, the formation of intermetallics through chemical vapor deposition (CVD) of semiconductors onto metal surfaces has received much less attention.[18−28] The present work illustrates that the controlling nature of the substrate on the sequential phase growth seen is markedly different from that evidenced on a Si single-crystalline substrate (where Si, rather than Pt, is in excess).

Our prior work on the Pt−Si system[29,30] examined growth and chemisorption properties on a Pt(111) substrate with Auger electron spectroscopy, low-energy electron diffraction (LEED), reflection absorption infrared spectroscopy (RAIRS), and temperature-programmed desorption (TPD). In that work we described (among other results) the discovery of seven ordered silicide phases. These phases correspond to multilayer structures that result from extensive interdiffusion of the Si into the Pt bulk. Of these phases, six directly reflect the hexagonal symmetry of the underlying Pt(111) lattice. Perhaps most interestingly, though, none of the latter structures could be assigned to structural motifs found for any of the known bulk platinum silicide phases.[31] These facts suggest two interesting questions for study: (a) what detailed atomic structures characterize the multilayer surface phases formed via the CVD-mediated growth and (b) what are the relative importances of the various structure-determining interactions (e.g. fcc metal substrate, thermal history, chemical identity of components, etc.) in this system. With regard to the former question, several possibilities exist. These include that the ordered phases observed with LEED and STM correspond to (a) a termination plane of a known bulk silicide phase, (b) the reconstruction of the surface of a known bulk silicide phase, and (c) a plane (reconstructed or not) of a novel silicide phase. The numerous hexagonal structures seen on Pt(111) suggest that this latter outcome is, in fact, quite important for the "inverted" CVD case. This possible epitaxy further suggests that the energetics associated with the geometric constraints imposed by the metal fcc(111) lattice, rather than the chemical nature of Pt, dominate the phase growth kinetics in the inverted Pt−Si system. To investigate these ideas further, we have performed and here present the results from a comparable study of the CVD of Si onto Pt(100). Our findings, derived from inferences gained from AES, LEED, and STM, provide a striking contrast to the phase growth seen on Pt(111),[29,30] Ni(100), and Ni(111) surfaces.[18,19,32] Our studies have found that a growth model based on a sequential phase evolution generally holds in this system. In contrast to the Pt(111) case, however, the phase evolution passes through at least two ordered, metastable phases that can be related to the structural motifs found in tetragonal bulk phases. A general discussion of the phase growth seen in the Pt−Si system by inverted CVD is presented.

II. Experimental Section

LEED and AES experiments were performed in a stainless steel ultrahigh vacuum (UHV) chamber with a base pressure of $<1 \times 10^{-10}$ Torr that has been described previously.[30] STM and additional AES experiments were performed in a second stainless steel ultrahigh vacuum (UHV) chamber with a base pressure of $<1 \times 10^{-10}$ Torr as described elsewhere.[29] Both chambers are equipped with cylindrical mirror analyzers and appropriate electronics (Physical Electronics) for Auger electron spectroscopy as well as ion guns (Phi) for Ar ion sputtering. LEED measurements were made with standard 4-grid optics (Physical Electronics). STM data were obtained with a Rasterscope 4000 Danish Micro Engineering A/S (DME; Herlev, Denmark) ultrahigh vacuum scanning tunneling microscope.

The Pt(100) crystals (one per chamber), purchased from Monocrystals Inc., were cut, oriented, and polished to within 0.5° with standard metallographic techniques. Heating was performed in the LEED chamber with a button heater in direct thermal contact with the crystal and in the STM chamber through e-beam bombardment of the back of the crystal. Cooling in both cases was effected through the introduction of cold gaseous or liquid nitrogen into a Cu reservoir that is held in direct contact with the sample-mounting hardware. Temperature measurements in the LEED chamber were made with use of a type K thermocouple spot-welded to the side of the crystal. As the crystal must remain transferable within the STM chamber, no direct temperature measurements were made, except at very high temperatures where an optical pyrometer was employed. Elsewhere, the temperature was estimated by using a type K thermocouple spot-welded to the sample-transfer coupon's mounting clip. As such, the temperatures quoted for the STM (but not LEED) data are estimates based on a calibration derived from data obtained by AES (shown in Figure 1).

The Pt crystals were cleaned with repeated cycles of room-temperature Ar (sputtering grade; MG Industries) ion sputtering followed by (as needed) heating in an oxygen (extra dry; MG Industries) ambient of $\sim 5 \times 10^{-8}$ Torr between 950 and 1000 K. The crystal was then annealed between 950 and 1100 K. The surface quality was assessed by AES in conjunction with either LEED or STM as available.

Silane (3% in UHP Ar; Matheson) was used as received and dosed from the background. Because large doses of the silane/Ar mixture were used, due to the high dilution, the exposures cited in the paper are estimates. We note that the dilute silane mixture allows for much safer handling than does pure silane.

All STM, AES, and LEED measurements were performed at room temperature (∼300 K) with the STM performed in height mode. The STM tips employed were PtIr purchased from DME and treated ex-situ only with an acetone wash. Tip cleaning in-situ was effected by using standard techniques[33] of bias and current ramping. The drift was typically found to be less than two nanometers over a 1 h period. All images are calibrated in x and y to a graphite standard and in z to Pt step heights. Image analysis was performed with Nanoscope (Digital Instruments) version 4.1 software after conversion from the DME image file format. All images are flattened and unfiltered unless otherwise noted.

(17) *Binary Alloy Phase Diagrams*, 2nd ed.; ASM International: Metals Park, OH, 1986; Vol. 2.
(18) Dubois, L. H.; Zegarski, B. R. *Surf. Sci.* **1988**, *204*, 113.
(19) Dubois, L. H.; Nuzzo, R. G. *Surf. Sci.* **1985**, *149*, 133.
(20) Sault, A. G.; Goodman, D. W. *Surf. Sci.* **1990**, *235*, 28.
(21) Dubois, L.; Nuzzo, R. G. *Langmuir* **1985**, *1*, 663.
(22) McCash, E. M.; Chesters, M. A.; Gardner, P.; Parker, S. F. *Surf. Sci.* **1990**, *225*, 273.
(23) Dubois, L. H.; Nuzzo, R. G. *Surf. Sci.* **1985**, *149*, 119.
(24) Dubois, L. H.; Zegarski, B. R. *J. Vac. Sci. Technol. A* **1988**, *6*, 870−874.
(25) Weigand, B. C.; Lohokare, S. P.; Nuzzo, R. G. *J. Phys. Chem.* **1993**, *97*, 11553.
(26) Hostetler, M. J.; Nuzzo, R. G.; Girolami, G. S. *J. Am. Chem. Soc.* **1994**, *116*, 11608.
(27) Lohokare, S. P.; Weigand, B. C.; Nuzzo, R. G. *Langmuir* **1995**, *11*, 3902.
(28) Kanazawa, T.; Kitajima, Y.; Yokiyama, T.; Yagi, S.; Imanishi, A. *Surf. Sci.* **1996**, *357−358*, 150.
(29) Bondos, J. C.; Gewirth, A. A.; Nuzzo, R. G. *J. Phys. Chem. B.* In press.
(30) Nashner, M. S.; Bondos, J. C.; Hostetler, M. J.; Gewirth, A. A.; Nuzzo, R. G. *J. Phys. Chem. B* **1998**, 102.
(31) *Pearson's Handbook of Crystallographic Data for Intermetallic Phases*, 2nd ed.; ASM International: Materials Park, OH, 1991; Vol. 4.
(32) Matsudaira, T.; Onchi, M. *J. Phys. C: Solid State Phys.* **1978**, 12.
(33) Chen, C. J. *Introduction to Scanning Tunneling Microscopy*; Oxford University Press: New York, 1993.

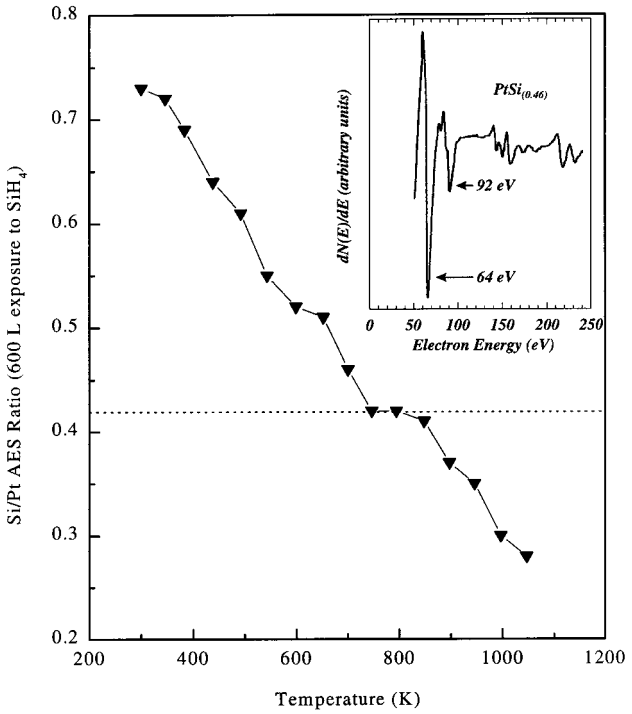

Figure 1. Evolution of the Auger spectra measured after separately flash annealing a silicon saturated Pt(100) surface to increasing temperatures. Saturation coverage was achieved by dosing 600 L silane at 300 K. The horizontal line is positioned to indicate the area where the presented curve's slope is zero. Inset: Auger electron spectrum for one representative silicide phase, $PtSi_{(0.46)}$. After dosing a saturation coverage of SiH_4 at room temperature, the Pt−Si surface was flash annealed to 850 K to yield this phase. The subscripted number is the AES ratio determined by direct measurement and ratioing of the peak-to-peak values for the Si (92 eV) and Pt (64 eV) transitions in the Auger spectrum.

III. Results

The results presented below define the nature of the phase evolution seen when Si is deposited onto Pt(100) via the thermolytic decomposition of SiH_4. A typical reaction sequence involved exposing the crystal to silane at 300 K until the uptake of Si was saturated (600 L). The coverages of Si reached in this way are actually quite large since, as data presented below show, interdiffusion within the near surface region is weakly activated. The structures described below thus correspond to multilayer arrangements of Si and Pt which progressively transform to increasingly Pt-rich forms during the thermal processing.

1. Auger Electron Spectroscopy. The AES data shown in Figure 1 demonstrate the compositional changes which occur as the Pt(100) crystal treated as described above is flash annealed in separate experiments to increasingly higher temperatures. The inset to this figure shows an Auger spectrum of a representative $PtSi_x$ phase in derivative mode. This particular spectrum was obtained after flash annealing a sample, one that had previously received a saturation exposure (600 L) of silane at 300 K, to the final temperature of 734 K. Among the several peaks observed, we note very intense peaks at 64 eV and a somewhat less intense peak at ca. 92 eV which are assigned to the Pt (NOO) and Si (LMM) transitions, respectively. The latter peak overlaps a weak Pt peak that occurs at approximately the same energy. The relative Si to Pt surface compositions were calculated from the ratio of the peak-to-peak distances for the 64 and 92 eV features. This quantity will be, hereafter, referred to as the Si/Pt AES ratio (x in $PtSi_x$). These ratios are not corrected for the Auger sensitivity factors because of the complicating effects of the peak overlap present at ca. 92 eV and the electronic effects that lead to the splitting of the 92 eV Si peak. For these reasons, the changes seen in the Si and Pt Auger ratios should be considered to be only qualitative indicators of the thermally induced evolution of the near surface composition.

For silane exposures made with the crystal held at ambient temperature, the maximum amount of Si that could be deposited onto the surface corresponds to an AES ratio of ∼0.75. This saturation limit was typically reached by using a 600 L exposure. The data presented below clearly establish that the surface is massively reconstructed in the presence of the Si, with the latter interdiffusing to a significant degree. Heating the sample after such an exposure depletes the near surface region of Si via continued solid−solid reaction and interdiffusion. The experiments described in this study examined surface phases with AES ratios in the range of about 0.75 to 0.24, the latter value being achieved through heating to 1097 K. It is interesting to note that lower SiH_4 exposures were necessary to saturate the Pt(111) surface (400 L).[30] This difference suggests that the diffusion energetics of Si through Pt may be asymmetric and sensitive to the face employed as the surface plane.

The temperature evolution of the $PtSi_x$ composition is seen in Figure 1. The AES data were measured after flash annealing a Si-modified surface to the indicated maximum temperature. Temperature-programmed reaction spectra (TPRS) showed that no Si-containing species desorb from the Pt surface during a heating cycle,[30] thus establishing that the reductions seen can only be ascribed to the interdiffusion of Si into the Pt bulk. The range of these atomic motions cannot be established, though, due to the finite AES penetration depth (electron mean free path of ∼6 Å at 92 eV).[34]

The data in Figure 1 show trends similar in qualitative terms to those seen for Pt(111).[30] On both substrates, heating depletes Si at the surface with this phase evolution showing regions of enhanced stability. It differs notably for Pt(100), though, in that there is only one clear plateau seen in the heating profile. As established for Pt(111),[30] these plateaus suggest a transition between intermediate silicide phases. As will be shown, there are, in fact, more phase transitions occurring in this system than is apparent from an inspection of the AES data above.

2. Low-Energy Electron Diffraction. To explore the thermal annealing profiles for regions where long-ranged order is present, we have examined the Si/Pt(100) system using low-energy electron diffraction (LEED). The evolution of the ordered LEED patterns[35] observed during the reaction of the deposited Si and the Pt(100) surface is shown in Figure 2 along with the corresponding Si/Pt AES ratios. Each pattern was recorded after flash annealing the Si/Pt(100) interface to the indicated temperature and subsequently cooling the sample to 300 K.

For reference, Figures 2a and 2b show the LEED patterns of the Pt(100)-(1×1) and the Pt(100)-(5×20) ("hex") surfaces, respectively. The latter was routinely obtained after the sputtering and annealing treatments outlined in the Experimental Section. The design of the chamber housing the LEED optics allows viewing only at opposing oblique angles and, thus, precludes photographing the entire LEED image. The LEED

(34) Somorjai, G. A. *Introduction to Surface Chemistry and Catalysis*; John Wiley & Sons: New York, 1994.

(35) The geometry of our chamber unfortunately does not allow us to take rearview images. We present in Figure 2 the largest field of view that our camera can capture ($>1/2$ of the pattern) and note for the reader that the half of the pattern which is not visible is completely consistent with the portion shown.

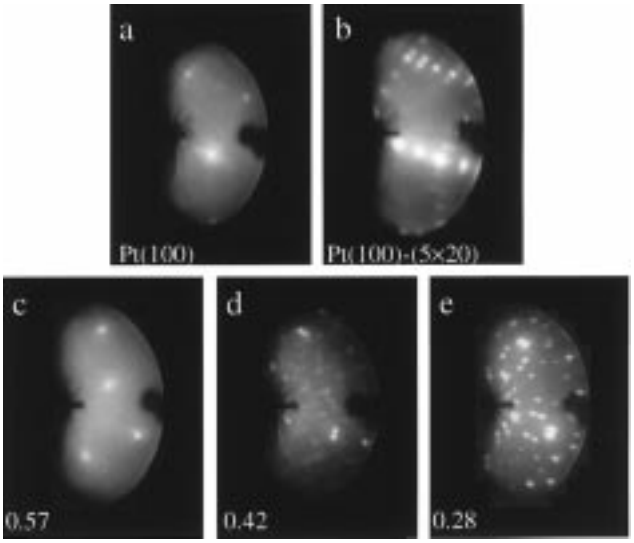

Figure 2. Low-energy electron diffraction (LEED) patterns measured at 300 K from (a) the Pt(100)-(1×1) surface, (b) the Pt(100)-(5×20) ("hex"), and (c−e) from silicide phases prepared by dosing a saturation coverage of Si at 300 K and then annealing. The AES ratios for the silicide phases are noted in the lower left-hand corners of each LEED pattern. The LEED optics in this chamber are viewed at an off-normal angle.

pattern obtained after saturation of the surface with silane but no subsequent flash anneal (a room-temperature anneal) yields a diffuse pattern (seen in Figure 2c) that is assignable to an overlayer of $(\sqrt{2}\times\sqrt{2})R45°$ symmetry (also referred to as c(2×2)). This pattern sharpens after a flash anneal to 346 K and persists for anneals ranging up to 652 K. The clarity of the patterns observed after flash annealing to temperatures >600 K diminishes significantly. The $\sqrt{2}$ pattern is lost after annealing to 700 K, although several very faint spots can be detected (AES ratio of 0.46). Flash annealing to even higher temperatures (746 to 997 K and AES ratios of 0.42 to 0.30, respectively) resulted in the new pattern shown in Figure 2d. This new pattern, for the 746 K anneal, is less intense than that seen for higher temperature processing in this range. The complex pattern shown in Figure 2d is composed of an extremely large number of spots which are aligned along a square Cartesian grid with the (0,0) LEED spot at the center. Of these spots only a small number are intense, but all are rather sharp. We have been unable to determine the Wood's or matrix notation for this pattern but suspect that it may be actually composed of several similar, overlaying LEED patterns. This interpretation is supported by the STM results presented below. The initial observation of this latter LEED pattern occurs at a temperature (and AES ratio) that correlates with the low-temperature side of the plateau seen in Figure 1. The decomposition of this phase is complete when the sample is annealed to temperatures >997 K (values higher than 1047 K were not investigated), whereupon a third pattern forms. This final pattern, shown in Figure 2e, is notable for its octagonal groupings of spots. This pattern is assigned to a $(\sqrt{17}\times\sqrt{17})R14.0°$ overlayer. We note that there are a few spots in this LEED pattern which do not correspond to a simple $\sqrt{17}$ overlayer. From this we must conclude that the overlayer is not a simple substitutional or adlayer structure. This inference also is consistent with the STM results presented below and the evolution of the AES results which clearly establish that this phase must be obtained as a result of an interdiffusion process. What is most intriguing is that the formation of this phase occurs in the absence of a clear plateau (Figure 1) or other compositional marker for this second phase transition.

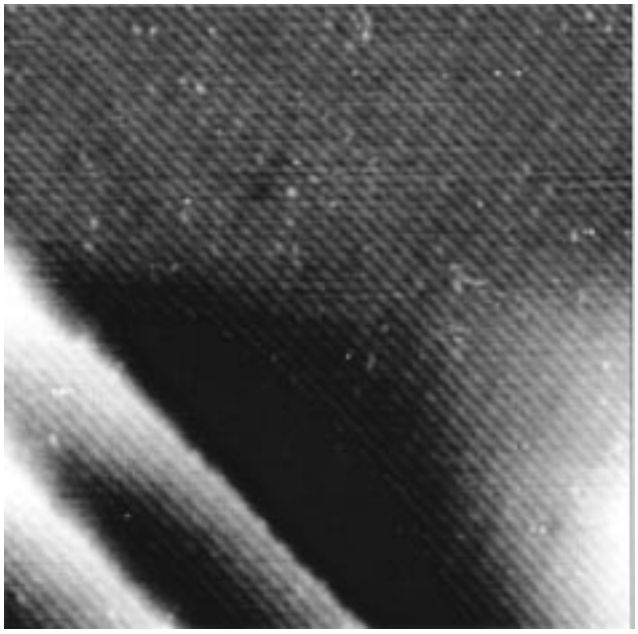

Figure 3. 75.5 by 75.5 nm scanning tunneling microscopy image of a bare Pt(100)-(5×20) ("hex") surface showing the overall step structure (two step edges in the lower left-hand corner; the large brighter and darker areas in this region are due to the flattening protocol). Note that the larger periodicity of the hex reconstruction is still visible. $V_{bias} = -100$ mV and $i_t = -0.40$ nA.

Aspects of the kinetics of the phase transition are unusual, though, in that it is gradual as evidenced by the appearance of coexistent LEED patterns at the lower end of its range of existence (temperatures of ~997 K).

The properties of the phases seen in the Si/Pt(100) system are relatively insensitive to the processing conditions. For example, dosing 600 L of silane with the substrate held at temperatures of 400 or 600 K also gave a $\sqrt{2}$ pattern, while dosing at 900 K resulted in the complex (middle temperature) pattern. Thus, dosing at an elevated temperature resulted in the same LEED pattern being observed as for an exposure made at 300 K followed by a flash anneal to that same maximum temperature. Additional experiments in which the maximum anneal temperature was held for 20 s at either ~400 or ~800 K gave the same phase as was obtained for flash anneals to those temperatures (where the hold time is ~0). Finally, LEED performed after sputtering and annealing at 1047 K sufficiently to give an AES ratio of 0.09 resulted in LEED spots for a $\sqrt{17}$ pattern.

3. Scanning Tunneling Microscopy. Scanning tunneling microscopy (STM) was employed to elucidate the detailed atomic positions and defect structures of the ordered silicide phases as well as the larger scale features (such as islands and facets) which might be present. The hexagonally reconstructed Pt(100)-(5×20) surface was first imaged for reference as shown in Figure 3. The surface was covered with parallel steps whose width varied from about 15 nm to over 100 nm with most steps being at least 50 nm wide. The parallel lines in this figure arise from the characteristic Pt(100)-(5×20) reconstruction.[36]

3.1. Large-Scale Images. Imaging of the Si-modified surface as a function of annealing temperature (or AES ratio) revealed distinct large-area trends in the evolution of the sample morphology as shown in Figure 4. For lower temperature anneals (e.g. AES ratio of 0.65; 421 K, not shown), the surface

(36) Behm, R. J.; Hosler, W.; Ritter, E.; Binnig, G. *Phys. Rev. Lett.* **1986**, *56*, 228.

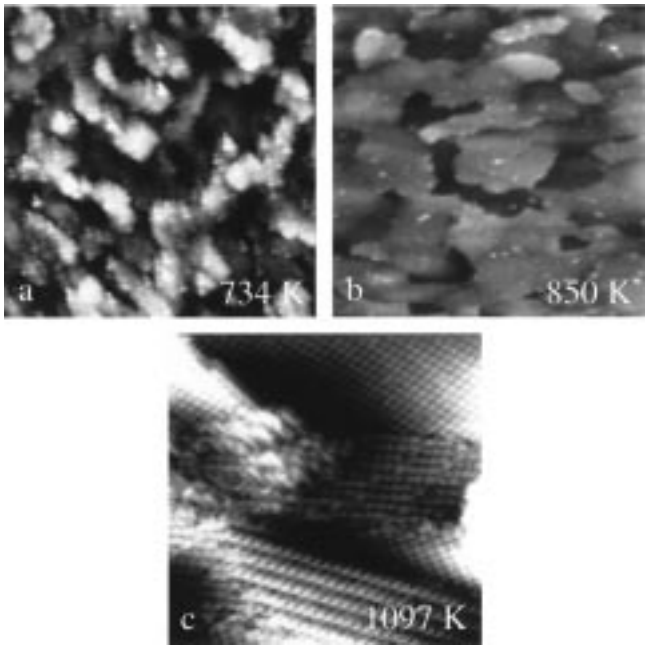

Figure 4. Representative scanning tunneling microscopy images collected after exposure of Pt(100) to 600 L of silane followed by flash anneals to 734, 850, and 1097 K with AES ratios of 0.46, 0.39, and 0.24, respectively (a−c): (a) 45.4 by 45.4 nm with $V_{bias} = 1.000$ V and $i_t = 0.33$ nA; (b) 54.4 by 54.4 with $V_{bias} = 0.500$ V and $i_t = 0.28$ nA; and (c) 34.3 by 34.3 nm with $V_{bias} = 0.297$ V and $i_t = 0.51$ nA.

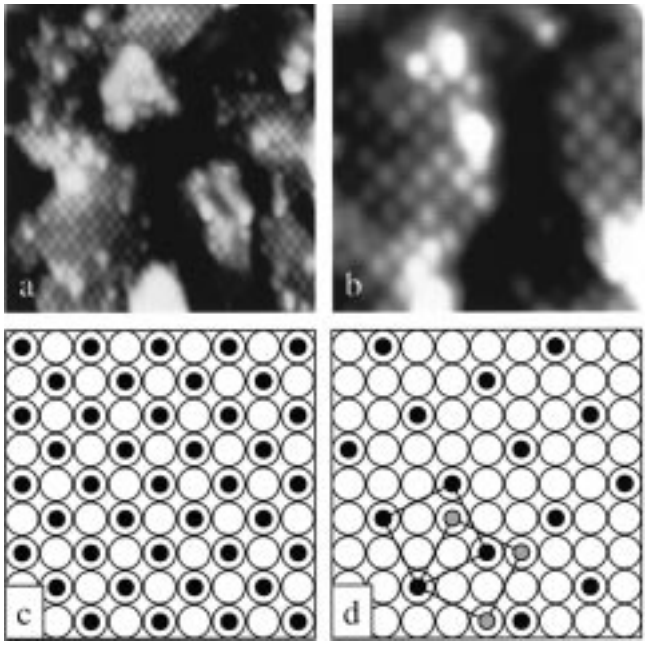

Figure 5. (a) An 11.4 nm by 11.4 nm STM image of the $(\sqrt{2}\times\sqrt{2})$-*R*45 overlayer ($V_{bias} = 0.707$ V and $i_t = 0.23$ nA) and (b) a 6.7 nm by 6.7 nm image of the $(\sqrt{5}\times\sqrt{5})R26.6$ overlayer ($V_{bias} = 0.707$ V and $i_t = 0.23$ nA). (c) The $(\sqrt{2}\times\sqrt{2})R45$ overlayer is shown schematically and (d) the $(\sqrt{5}\times\sqrt{5})R26.6$ overlayer shown schematically with a surface unit cell outlined in black as well as a surface unit cell formed from the opposite rotation. Atop sites were chosen simply for clarity.

is covered with very small, irregular islands; the island sizes obtained increase directly with the annealing temperature as shown in the comparison between Figures 4a and 4b. The height differences between adjacent islands in the surface normal direction in all cases are generally from one to three times the Pt(100) step height. When annealed past 1000 K (AES ratio of 0.30) the restructuring produced terraces that were more than 100 nm in size. The original surface steps are not discernible in any of the treated samples. It is also notable that the surfaces of the highest temperature phases (over 1000 K, Figure 4c) exhibit substantial step bunching (up to ∼9 steps) resulting in the production of local facets and larger islands. The general roughness of these phases contrasts greatly with the extreme flatness of the bare Pt(100) surface (Figure 3) and attests to the substantial restructuring of the substrate that accompanies the phase growth.

3.2. Short-Range Images. We did not obtain atomic resolution from silicide phases with an AES ratio of 0.65 (421 K). Phases with this AES ratio did, however, evidence a diffuse $\sqrt{2}$ LEED pattern. This suggests that the topmost layer in this material is disordered. The presence of the c(2×2) LEED pattern at these conditions, however, suggests the presence of, at least, subsurface (perhaps second layer) order of that type.

3.2.1. $\sqrt{2}$ and $\sqrt{5}$ Structures. Annealing to a slightly higher temperature (454 K; AES ratio of 0.63) results in an ordered, imagable overlayer covering the vast majority of the sample surface. This overlayer is square with a nearest neighbor distance of 0.39 ± 0.02 nm as shown in Figure 5a. No rotated domains were found. The symmetry and atomic separation is in excellent agreement with the value of 0.392 nm that is expected for a $(\sqrt{2}\times\sqrt{2})R45°$ overlayer on Pt(100). This overlayer, shown schematically in Figure 5c, is observable for a large range of annealing temperatures up to 734 K (AES ratio of 0.46).

At and above this higher temperature, however, there exists another coexistent overlayer also of square symmetry. A representative image of this new structure is shown in Figure 5b. The interatomic spacing seen in this image is 0.60 ± 0.02 nm with an angle between rotated domains of 53 ± 2°. This corresponds closely with the symmetry and spacings expected for a $(\sqrt{5}\times\sqrt{5})R26.6°$ overlayer (interatomic spacing of 0.619 nm and an interdomain angle of 53.1°). The structure of a $\sqrt{5}$ overlayer with both possible rotated domains is shown schematically in Figure 5d. The $\sqrt{5}$ structure is only observed over a narrow range of temperatures and Si concentrations (temperatures between ∼730 and 850 K and AES ratios of 0.46 to 0.39, respectively). At 800 K the $\sqrt{5}$ overlayer is found on a minority of the islands (and only those that are not topmost in the *z* direction) with the others exhibiting no discernible atomic level order. This finding correlates with an almost complete elimination of long-ranged order, as deduced by LEED, at similar temperatures.[37]

For both square symmetry overlayers, the islands observed stay relatively small with many islands not exceeding 10 nm in width. These islands are also irregular in shape. We further found that the individual islands lacked internal domain boundaries, although in the $\sqrt{5}$ case different domains could be found on different islands. Also, for both overlayers, there exist isolated areas where the overlayer experiences small *z* height depressions up to ∼5 atoms wide. These features have a corrugation of two to three times the overlayer's corrugation height (much smaller than a step height) and are attributed to the procession of the overlayer over a subsurface vacancy or collection of vacancies.

The fact that the $\sqrt{5}$ overlayer was not detected by LEED is likely due to three factors. First, the temperature range for its existence is very small. Second, the island size is also very small. Third, the $\sqrt{5}$ phase is often a minority phase. At island sizes below ∼10 nm, LEED patterns start to become faint and diffuse due to the low number of diffraction events contributing per

(37) Minor variances between STM and LEED transition temperatures are attributed to the differences between the different heating methods and temperature measurement procedures used.

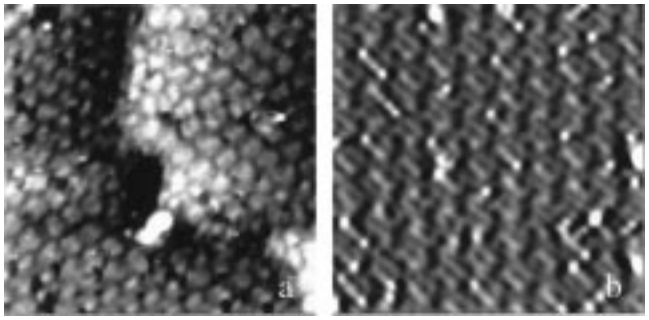

Figure 6. (a) A 18.0 nm by 18.0 nm representative image of the quasihexagonal overlayer on two adjacent steps ($V_{bias} = -0.250$ V and $i_t = -0.28$ nA) and (b) a 11.4 nm by 11.4 nm image of the same overlayer (not the same area) that has been subjected to a Gaussian high-pass filter to emphasize local structure.

domain.[38] This effect is greater for overlayers with larger unit cells and, thus, would be worse for a $\sqrt{5}$ than a $\sqrt{2}$ overlayer. It is not altogether surprising, then, that this $\sqrt{5}$ pattern was not detected by LEED.

3.2.2. Quasihexagonal Structure. At temperatures of 850 to 998 K (AES ratios of 0.39 to 0.30; conditions for the formation of the complex LEED pattern) STM shows that another ordered overlayer is formed. This overlayer consists of a quasihexagonal array of atomic groupings with average distances between the groupings of 1.28, 1.47, and 1.38 ± 0.02 nm in the three primary directions as shown in Figure 6a. The average angles between primary directions are 53, 67, and 60 ± 2°. These distances and angles do not allow for the construction of a Wood's notation using either high or lower symmetry (bridge in addition to 4-fold hollows and atop sites) sites. One striking feature of the structure revealed in this image is the tight convolution of several domain boundaries (between small domains) and a substantial population of void structures. It appears that, together, these effects act to produce many small domains of slightly different local symmetry. These domains tend to increase in size with increasing annealing temperature.

The atomic groupings which compose the quasihexagonal array components appear to consist of six, three, or (ordinarily) four protrusions, as can be seen in the image presented in Figure 6b (a Gaussian high-pass filter was applied to this image to emphasize the local ordering). In many cases it is found that two of these protrusions are brighter by STM than the others in the examined grouping. These protrusions appear to form a variety of convex shapes with an average interatomic distance of 0.58 ± 0.02 nm. We presently do not completely understand the nature of these atomic arrangements or the nature of the spacing(s) observed (which on the average fall midway between the separations expected for $\sqrt{4}$ and $\sqrt{5}$ spacings). Additionally, this structure exhibits a significant *z* corrugation of ∼0.04 nm between brightest and darkest items in this image with the distances in *z* between brightest and middle and between middle and darkest being about the same. Whatever its nature, this structure is easily formed, persistent, and independent of the tip used. For example, a silane exposure performed at ∼700 K[39] (AES ratio of 0.43) gave the same overlayer architecture (albeit with slightly larger than average islands). Heating eventually leads to the elimination of this structural phase at temperatures >998 K.

3.2.3. $\sqrt{17}$ Structure. This latter transition leads to the formation of the fourth distinct ordered overlayer characterized in this work. An example of an STM image of this phase is shown in Figure 7a. This surface (AES ratio of 0.30) presents a square array of large, oblong protrusions forming a "pinwheel pattern". The apparent distance separating the bright bars is 1.15 ± 0.02 nm with an angle between rotated domains of 29 ± 2 degrees. These numbers are good matches for the 1.142 nm and 28.1° between rotated domains expected for the ($\sqrt{17}\times\sqrt{17}$)-*R*14.0° overlayer seen by LEED. A schematic description of the cell structure is shown in Figure 7c (the thick black line segments correspond to the bright bars). The length of the bright bars is ∼0.61 nm, which corresponds to a $\sqrt{5}$ distance. A closer inspection of Figures 7a and 7b reveals that each oblong protrusion is centered (slightly off-diagonal) in a square (middle gray) feature that is surrounded with even lower features (darkest gray). The corrugation in this three-level image is the same as is found for the quasihexagonal pattern. Most intriguingly though, one finds in several places in the images adatoms which are adsorbed at the centers (area pointed to by four oblongs; **x** in Figures 7b and 7c) of the pinwheels but never between them (**y** in Figures 7b and 7c). This correlation of the adatom placement sensitivity was confirmed in replicate experiments and we conclude that it is an essential feature of the multilayer silicide structure whose nature is described in detail below. The STM imaging shows a mild bias dependence with a more elongated version of the oblongs (Figure 7b) being obtained at biases above 0.7 V and a less elongated version (Figure 7a) occurring at lower (or negative) biases. We have never achieved sufficient resolution on the oblong features to identify possible atomic constituents or positions.

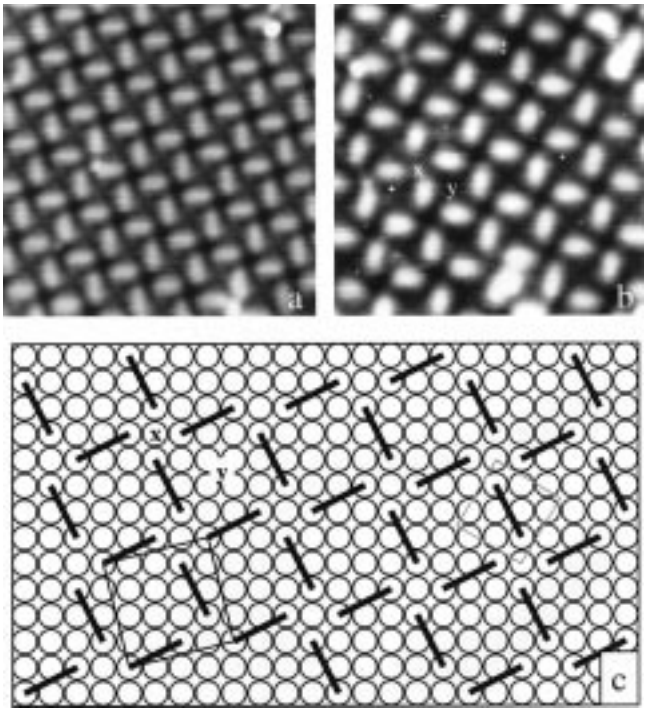

Figure 7. (a) A representative 11.4 nm by 11.4 nm STM image of the ($\sqrt{17}\times\sqrt{17}$)*R*14.0 overlayer at low bias ($V_{bias} = -0.500$ V and $i_t = -0.28$ nA) and (b) a representative 9.2 nm by 9.2 nm STM image of the same overlayer (not same area) at high bias ($V_{bias} = 0.707$ V and $i_t = 0.28$ nA). This overlayer is shown schematically in part c along with a version of its surface unit cell (square in the lower left corner). The bright, oblong protrusions are represented by thick black lines and the middle-gray squares seen in parts a and b are outlined by the square on the right side. The letter **x** corresponds to an occupyable site indicated by the same letter in part b and the letter **y** indicates the unoccupyable site indicated by the same letter in part b. Again atop sites were chosen for clarity.

(38) Somorjai, G. A. *Chemistry in Two Dimensions: Surfaces*; Cornell University Press: Ithaca, 1981.

(39) This value was measured with an optical pyrometer.

The schematic depiction shown in Figure 7c shows one possible domain of a $\sqrt{17}$ overlayer with a pinwheel architecture that reflects structural elements seen in the STM images presented in Figures 7a and 7b. It is notable that, for this arrangement, the sites that correspond to the centroids of the squares and pinwheels align with distinct high-symmetry sites. We caution that this correspondence should not be overly interpreted. This phase is not an adlayer structure, and while such correspondences are no doubt important interactions governing the apparent epitaxy, they need not precisely correlate with the surface corrugation seen by STM. The nature of this multilayer structure is discussed in detail below.

IV. Discussion

We have presented AES, LEED, and STM data which illustrate the nature of the structures which result from the chemical vapor deposition of Si onto Pt(100) with silane as the Si source. The LEED and STM results are highly consistent, revealing $(\sqrt{2}\times\sqrt{2})R45°$ overlayers in the same region of the compositional phase space. They also both reveal a complicated (and what is, as yet, incompletely understood) quasihexagonal structure in a region of phase space that is highly defected and may consist of a coexistent combination of several similar structures. Both techniques demonstrate that growth at high temperatures leads to the formation of a Pt-rich phase that can be indexed as a $(\sqrt{17}\times\sqrt{17})R14.0°$ overlayer. Additionally, the STM revealed a $(\sqrt{5}\times\sqrt{5})R26.6°$ structure existing at the end of the compositional phase space for the $\sqrt{2}$ structure that was not seen by LEED. The formation and decomposition of these phases proceeds by solid−solid reactions mediated by the dynamics of interdiffusion in the near surface boundary layers. In the discussion that follows, we will present an overview of the reactions seen and present models which relate the apparent epitaxy to the known structural chemistries of Pt−Si intermetallic phases.

The clearest connection with known structural chemistries of the Pt−Si binary system follows from an understanding of the composition of the surface boundary layer films. The Pt−Si binary system presents a complex phase diagram, showing no fewer than eight stable binary phases.[17] Additionally, at least sixteen Pt−Si bulk structural phases have been characterized with use of X-ray methods, not all of which are stable.[31] The experiments performed in this study correspond to growth occurring in the presence of an extremely large excess of Pt. In fact, the quantity of Si present is sufficiently low that it is not possible to saturate the low solubility of Si in Pt. The phase growth, then, must reflect the nature of the kinetics/dynamics involved in atomic diffusion as mediated by intermediate compound formation and decomposition. The ordered structures seen here clearly establish that metastable phases, with structures showing apparent epitaxial correspondences to the Pt(100) substrate, are important intermediates. One wonders, then, whether these phases can be directly correlated with known Pt−Si bulk phases. As noted above, compositional information provides a convenient starting point to look for such correspondences. The connection of the AES results to such bulk structural information is, however, a complicated process. AES has a finite penetration depth of ~6 Å for the transitions studied here and, thus, averages over a few atomic layers of the structures. The data clearly show that with increasing temperatures, the Si/Pt ratio decreases, a result that must be attributed to Si diffusion into the Pt bulk. This decrease in Si content of the near surface region is more broadly correlated with an increase of the surface unit cell area for the transitional, metastable phases. With the exception of the single plateau seen at the formation of the quasihexagonal structure, the composition as evaluated with AES appears to change continuously throughout the compositional phase space investigated. We believe part of this behavior originates from the extreme restructuring of the substrate, both atomistically and on larger scales, which accompanies the phase development. It is clear that the phases formed become increasingly Pt-rich, ranging in compositions slightly above that expected for PtSi to phases that may actually be more metal rich than Pt_2Si (and fairly near to Pt_3Si). The literature suggests that both Pt_2Si and Pt_3Si are important intermediate or terminal phases for compound growth by interdiffusion when the supply of Si is limited.[7]

In the present data we see (from LEED and STM) the following pattern of phase formation. By increasing the annealing temperature, the surface structures transform progressively from $\sqrt{2}$, to $\sqrt{5}$, to quasihexagonal, and, ultimately, to the complex $\sqrt{17}$ overlayer. The data do not allow us to make an assignment of a surface atomic concentration to any of the structures seen by STM as we do not know how many atoms comprise the unit cells or which ones are Si or Pt and where they reside in the multilayer structure. One could provide speculative atomic concentrations for the topmost layers of the $\sqrt{2}$ and $\sqrt{5}$ overlayers, but such a number would not allow for direct correlation with the AES results as it ignores the multilayer nature of these structures.

A primary conclusion of our earlier Si/Pt(111) work was that none of the many overlayers observed had any direct structural relationship to the known Pt silicide phases. This follows from the fact that the hexagonal symmetry of the overlayers does not map well onto the tetragonal and orthorhombic symmetries characterizing many of the known phases (and the measured lengths and atomic positions in the phases found on Pt(111) are a poor match for the few known hexagonal phases). The same cannot be said for the square symmetries of the overlayers forming on Pt(100). We start with a consideration of the $(\sqrt{2}\times\sqrt{2})R45°$ overlayer.

1. $\sqrt{2}$ Phase. Correspondence with the Pt(100) plane is accommodated by several known phases of Pt_2Si and Pt_3Si. The well-known H_2Th structure (Pearson symbol of tI6)[40] found for some types of Pt_2Si, the structure of which is in Figure 8, provides one structural model for this overlayer.[31] In this structure (looking along the *c* axis) one finds a layer of Si atoms in a square array with an interatomic (a parameter) distance of 0.3948 or 0.3933 nm (for the two different bulk phases which assume this structure).[31] These latter values are in line with the ideal $\sqrt{2}$ distance of 0.3917 nm and our measured value of 0.39 nm. The layer below the topmost layer in this Pt_2Si structure is a square array of Pt atoms that are rotated 45° (and are $\sqrt{2}$ smaller than the upper layer). The next layer is comprised of a single Si atom in the center of the cell followed by a Pt layer identical with the earlier one, and finally, a Si layer identical with the first (the tetragonal cell has inversion symmetry). The first two levels of this structure, thus, transpose as a simple Si $\sqrt{2}$ adlayer on Pt(100). Thus, although there is a strong correlation between our surface and two bulk phases we cannot assert that they are the same since a basic adlayer structure would look identical to the top of a bulk phase.

We can find an alternative correlation between the $(\sqrt{2}\times\sqrt{2})R45°$ structure and the SiU_3 (Pearson symbol tI16)[40] structural form of Pt_3Si (it is interesting to note that both Pt and U silicides

(40) Daams, J. L. C.; Villars, P.; van Vucht, J. H. N. *Atlas of Crystal Structure Types for Intermetallic Phases*; ASM International: Materials Park, 1991; Vol. 3.

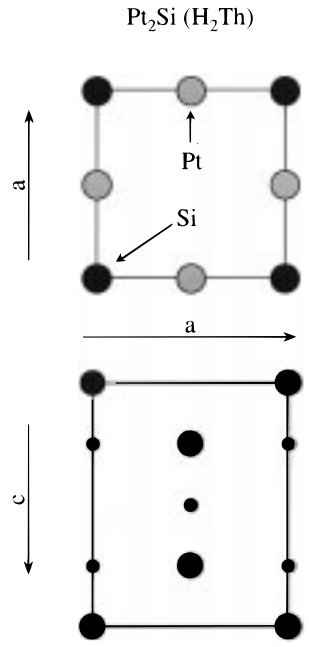

Figure 8. Top and side views of the tetragonal unit cell for the types of Pt_2Si which assume the H_2Th structure.[40] Pt is shown in gray and Si in black. For these types of Pt_2Si $a = 0.3933$ nm and $c = 0.5910$ nm or $a = 0.3948$ and $c = 0.5963$ (there are two different known types of Pt_2Si with this structure).[31] Note that the *a* parameter is a very good match for a $\sqrt{2}$ distance on Pt(100).

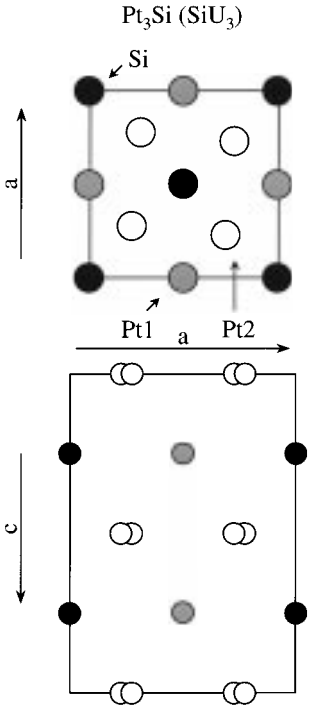

Figure 9. Top and side views of the tetragonal unit cell for the type of Pt_3Si that assumes the SiU_3 structure.[40] The two types of Pt are shown in gray and white and Si is shown in black. For this type of Pt_3Si $a = 0.546$ nm and $c = 0.786$ nm.[31]

assume the same basic structural type).[31] This Pt silicide phase (Si assigned to Si and Pt to U) consists of a five-layer structure as shown in Figure 9. The first layer (proceeding down the *c* axis) is comprised of an inner core of Pt atoms in a square array. The second layer is comprised of $(\sqrt{2}\times\sqrt{2})R45°$ arrays of Si and Pt which interpenetrate as in the NaCl structure. The third layer is a layer of Pt similar to the first followed by another interpenetrating $\sqrt{2}$, Pt−Si layer that is, in turn, followed by a third layer of Pt. Five layers are required as the first, third, and fifth layers (all Pt) are rotated slightly from the ideal 4-fold hollow positions in the interpenetrating layers (the first and fifth counterclockwise and the third clockwise; see the figure). The spacing between Si and Pt atoms in the interpenetrating layers is 0.3861 nm, which again is very close to the $\sqrt{2}$ distance. If one takes the second and third layers, one finds a $(\sqrt{2}\times\sqrt{2})$-$R45°$ overlayer with Si in substitutional sites on top of a slightly rotated Pt(100) layer. This model, thus, also may serve to rationalize the structural nature of the $(\sqrt{2}\times\sqrt{2})R45°$ overlayer seen in this work. We cannot be certain whether the imaged overlayer is an adlayer or substitutional layer or even a multilayer compound phase as we cannot see the underlying layers. Even so, we believe that the H_2Th structure is a better structural model due to the fact that the stoichiometry of Pt_2Si is a better match for the AES ratios than is Pt_3Si.

2. $\sqrt{5}$ Phase. Investigation of the known bulk Pt silicide phases does not reveal a structure that would serve as a suitable model for the $\sqrt{5}$ overlayer pattern. It is likely, however, that this overlayer is a transient metastable phase formed when the $\sqrt{2}$ overlayer loses a critical density of surface Si via interdiffusion. This argument is in accord with the relatively small area of compositional phase space where this overlayer is found. We have also been unable to find a known bulk material that would suitably model the quasihexagonal phase through cleaving the unit cell at a low index plane. A model for the $\sqrt{17}$ phase (discussed below) does provide a basis for understanding some of the structural motifs seen in this layer, however.

3. $\sqrt{17}$ Phase. The $(\sqrt{17}\times\sqrt{17})R14.0°$ structure is a Pt-rich phase. No known Pt_3Si structures appear to be able to model the unique surface motifs or spacings seen for this compound layer. However, a suitable model can be found in one Pt-rich bulk phase, $Pt_{12}Si_5$, which assumes the $Ni_{12}P_5$ (Pearson symbol tI34) structure.[40] This structure is a complex five-layer architecture shown in Figure 10 of which we will only discuss the top two layers ((100) and the one below that along *c*). The (100) plane is a distorted square array that alternates between Pt and Si in a method similar to a distorted NaCl lattice but with a vacancy in the center of the unit cell (**x** in this figure). Below that layer resides a distorted square array of Pt, with the Pt placed so as to approximately reside at 4-fold hollow sites of the upper layer. If the unit cell is tiled four or more times, an interesting motif is evident. If adjacent (closest) Pt or Si atoms (but not both) are paired (there are two types of Si atoms in this cell which are called types 1 and 2; it is the type 2 Si's that are paired)[40] in the topmost layer, one obtains a pinwheel motif very similar to that seen in the $\sqrt{17}$ overlayer. In this motif the pairs (which correspond to the $\sqrt{17}$ oblongs) are centered in squares formed by type 1 Si's and the vacancies mentioned above (two of each per square, as shown in Figure 10). These squares are very similar the one shown on the right side of Figure 7c, which is also defined by a half occupancy each of atop sites and 4-fold hollows. In the $Pt_{12}Si_5$ structure, these pairs define a direction that is rotated slightly from the diagonal of the square grouping just mentioned, as are the oblongs in the $\sqrt{17}$ overlayer images. We cannot make a direct equivalence between the distances seen in the images, however, and the unit cell size for the bulk Pt−Si structure. This latter unit cell is smaller than that seen by STM (the overall bulk cell size is closer to a $\sqrt{13}$ distance than $\sqrt{17}$ and the oblongs are somewhat smaller than an ideal $\sqrt{5}$ length). Furthermore, this bulk cell does not scale evenly onto the $\sqrt{17}$ overlayer. Finally, the Si/Pt ratio of 0.42 is also apparently too high for the AES ratios measured for the $\sqrt{17}$ overlayer.

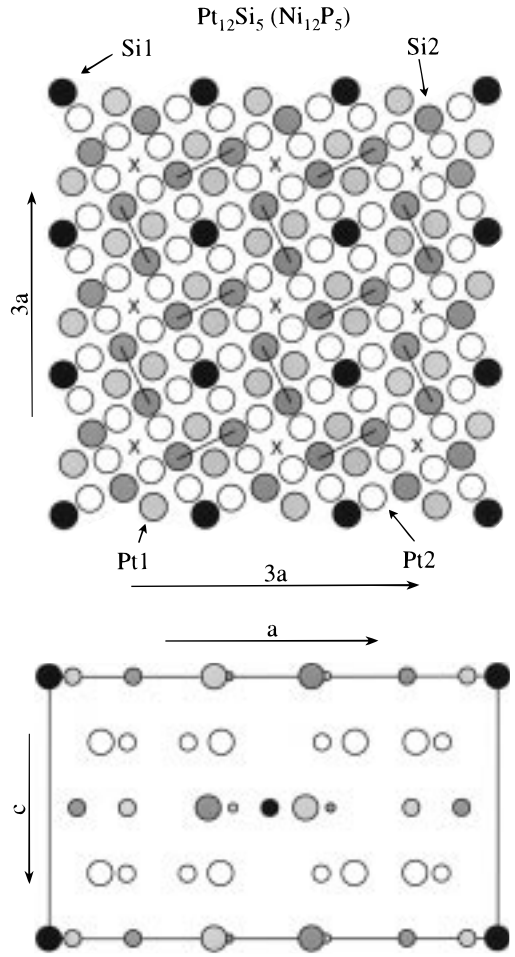

Figure 10. Top and side views of the tetragonal unit cell for the type of $Pt_{12}Si_5$ that assumes the $Ni_{12}P_5$ structure.[40] The two types of Pt are shown in light gray and white and the two types of Si in darker gray and black. For this type of $Pt_{12}Si_5$ $a = 0.9607$ nm and $c = 0.5542$ nm.[31] For the top view, the unit cell has been tiled nine times and adjacent gray Si (type 2) have been connected to present the pinwheel structure.

Four complicating issues need to be considered when evaluating such matters. First, the STM measures electron density of the entire surface and not actually the precise positions of the atoms. These two items need not be identical. Second, the AES values do not take account of the obvious splitting seen at the low-energy side of the Si LMM transition, which is significant for all observed phases on Pt(100). Third, we do not know the complete character of the diffusional profile (across the top part of which the AES averages) which leads to its formation. Fourth, the abrupt termination of the $Pt_{12}Si_5$ lattice does provide a significant rationalization for atomic relaxations or reconstructions of the surface atoms. Even so, we note certain characteristics of the Ni−P cell that map very well onto the $\sqrt{17}$ Pt−Si overlayer. First, if we assume that the oblongs correspond, at least in part, to paired Si atoms, then the pinwheel center sites (which can be occupied in the $\sqrt{17}$ structure) are the aforementioned vacancies (**x** in Figure 10) while the between sites (which are not occupied in the $\sqrt{17}$ structure) are filled by type 1 Si atoms. If true, then only one type of Si is being imaged by STM. The converse, where the oblongs are formed by paired Pt atoms, is a less enticing argument although still conceivable upon consideration of Figure 10 (the pinwheels would center on filled sites while the unoccupyable sites are empty). We conclude from the image bias dependence that the oblongs are most likely Si atoms that may also have electron density contributions from nearby Pt or other Si atoms. Second, the occupyable and unoccupyable sites (type 1 Si and vacancies) are surrounded most closely by Pt atoms. This is also true of the other Si atoms (type 2). The converse, however, is not true (Pt has close Pt and Si neighbors). This is in accord with the covalent nature of Ni phosphides and Pt silicides where the minority element is often surrounded by the majority species.

Taken together, the arguments given above suggest that there is a strong but not necessary correlation between the $\sqrt{2}$ overlayer and known Pt_2Si structures and an intriguing correlation between the $\sqrt{17}$ overlayer and a bulk $Pt_{12}Si_5$ structure. We, therefore, conclude that the thin film intermetallic overlayers formed by the inverted CVD of Si onto Pt(100) with silane are more strongly correlated with bulk silicide structures than those formed on Pt(111). There does not exist a Si/Pt overlayer, though, that can only be rationalized based on the imaging of a known bulk phase. The $\sqrt{17}$ overlayer provides an interesting suggestion that such effects are important, but the data are not completely convincing. Direct imaging of the atoms in this overlayer could provide such evidence (especially if they were altered from their ideal positions in a manner dictated by the $Ni_{12}P_5$ structure), but to this point we have not obtained the resolution necessary to prove this. The issue of the origin of the overlayers is, thus, still somewhat unclear. At least some Si/Pt overlayers are unrelated to the bulk structures if for no other reason than there are more hexagonal overlayers found on Pt(111) than there are known hexagonal bulk phases.

4. Quasihexagonal Phase. Building on the insights gained from the $Pt_{12}Si_5$ model for the $\sqrt{17}$ structure, a careful study of the quasihexagonal overlayer reveals several similarities with this overlayer. First, the quasihexagonal structure, as with the $\sqrt{17}$ overlayer, has at least a three-level surface structure. Both have similar corrugation heights composed (mostly) of rectangles with bright protrusions crossing them (the rectangles) which are approximately $\sqrt{5}$ in length. Also, they both have similar atomic densities. More importantly, though, both form as coexistent phases over a modest range of annealing temperatures. When one considers the fact that the quasihexagonal structure has an overall large level of disorder, it seems reasonable to conclude that the quasihexagonal structure may actually be a highly defected, transient version of the $\sqrt{17}$ structure that converts to the more ordered form when the temperature becomes high enough to allow for the necessary surface diffusion and domain coarsening. Since both overlayers are composed of rectangular units it is likely that the atomic motions required for the interconversion are complex and possibly concerted.

5. Correlation with Other Intermetallic Phases. We now turn to a consideration of the relationships of these results to those reported for other intermetallic phases. Of the overlayer structures that we have identified in this study, there is literature precedent only for the $(\sqrt{2}\times\sqrt{2})R45°$ overlayer in a transition metal silicide system namely for Co and Fe on Si(100)[41] and for Si/Ni(100).[18,32] Looking more broadly, though, we note that of the structures observed on Pt(111), only the $(\sqrt{3}\times\sqrt{3})R30°$ and $(\sqrt{19}\times\sqrt{19})R23.4°$ overlayers were reported on other Si on metal fcc(111) surfaces (on Ni[19] and Cu[22,25] for $\sqrt{3}$ and on Pt[42] for $\sqrt{19}$). Thus, the correspondence between overlayers observed for Si/Ni and Si/Pt, regardless of face, is only for the smallest non-(1×1) commensurate structures possible for the

(41) Lifshits, V. G.; Saranin, A. A.; Zotov, A. V. *Surface Phases on Silicon. Preparation, Structures, and Properties*; John Wiley & Sons: New York, 1994.

(42) Diebold, U.; Zhang, L.; Anderson, J. F.; Mrozek, P. *J. Vac. Sci. Technol. A* **1996**, *14*, 1649.

given face. The larger unit cell structures seen on Pt including a $(6\sqrt{2}\times6\sqrt{2})R45$ pattern observed by Cardillo by LEED[43] were not seen on Ni. This last structure was not observed by us probably due to the very different formation procedures (silane CVD versus impurity segregation) and the fact that Cardillo's AES ratio (0.22) was lower than any probed by us in these studies. Similarly, the p(2×2) LEED pattern seen on Ni(111)[19] and the $(2\sqrt{2}\times\sqrt{2})R45$ pattern observed on Ni(100)[32] were not identified on the respective Pt faces. This suggests that the chemical identity of the metal is an important consideration in overlayer structure formation especially at lower Si concentrations. At the higher Si concentration the overlayer correspondence is most likely a result of packing considerations (large Si density and the preference for high-symmetry sites). This lack of correspondence is not surprising considering that Ni and Pt form silicides that are fundamentally different (i.e. Ni forms Si-rich silicides and Pt forms Pt-rich silicides).[1−3] A better comparison would be between Pd and Pt, but the Pd(111) and Pd(100) information is not currently available in the literature. However, the fact that all but two of the overlayers seen on Ni or Pt (namely, the rectangular overlayer on Pt(111)[29] and the quasihexagonal overlayer in this work) are commensurate and directly reflect the substrate's overall lattice symmetry (hexagonal or square) indicates that substrate direction from the transition metal fcc face is highly important. Further evidence for this comes from the large number of overlayers on Pt that are independent (or may be independent) of the structural motifs formed for bulk phases, namely all of the Si/Pt(111) and some of the Si/Pt(100) overlayers. Notably, but not surprisingly, no overlayers were formed that are common to the (111) and (100) faces of either Ni or Pt.

Finally, it should be noted that there are several characteristics of the Si/Pt(100) system that are common to the Si/Pt(111) system. First, the surface is completely covered with small irregular islands upon low-temperature anneals, and these islands grow in size with increasing temperature. There is not a critical temperature for the (100) system at which the islands disappear; instead, they continue to grow throughout the temperature range that we have explored. Second, the $\sqrt{2}$ phase becomes unstable at sufficiently high temperatures due to a lack of surface Si, yielding the $\sqrt{5}$ phase, which at higher temperatures is replaced by a largely disordered surface. This type of phase termination due to loss of Si to diffusion is a central result of the (111) studies and also is in agreement with work on Si/Pd(110).[44,45] The expected decomposition of the $\sqrt{17}$ phase was not observed, most likely due to the maximum temperature used in these studies being too low. Third, we have observed coexistent phases on Pt(100) at two phase boundaries. This behavior is similar to the coexistences observed on the (111) face and implicitly confirms the strong mediating role played by transport in these transitions. One difference seen in our data is that the silicides formed on Pt(100) apparently have greater stability than those formed on Pt(111). An asymmetric facility for diffusion may underlie this latter observation of the relative energetics of the degradation and formation behaviors. Further work will be needed to clarify this point.

Acknowledgment. This work was funded by the Department of Energy (DEFG02-91ER45439) through the University of Illinois Frederick Seitz Materials Research Laboratory and by the National Science Foundation (CHE9626871). J.C.B. acknowledges financial support via fellowship awards from the National Science Foundation.

JA9828511

(43) Cardillo, M. J.; Becker, G. E. *Surf. Sci.* **1980**, *99*, 269.
(44) Wälchli, N.; Kampshoff, E.; Kern, K. *Surf. Sci.* **1996**, *368*, 258.
(45) Wälchli, N.; Kampshoff, E.; Menck, A.; Kern, K. *Surf. Sci.* **1997**, *382*, L705.